NRL Report 8012

VHF-UHF Aircraft Antenna

FREDERICK FINE

Aerospace Systems Branch
Space Systems Division

July 23, 1976

NAVAL RESEARCH LABORATORY
Washington, D.C.

SECURITY CLASSIFICATION OF THIS PAGE *(When Data Entered)*

REPORT DOCUMENTATION PAGE		READ INSTRUCTIONS BEFORE COMPLETING FORM
1. REPORT NUMBER NRL Report 8012	2. GOVT ACCESSION NO.	3. RECIPIENT'S CATALOG NUMBER
4. TITLE *(and Subtitle)* VHF-UHF AIRCRAFT ANTENNA		5. TYPE OF REPORT & PERIOD COVERED Final Report 6. PERFORMING ORG. REPORT NUMBER
7. AUTHOR*(s)* Frederick Fine		8. CONTRACT OR GRANT NUMBER*(s)* NRL Problem R07-35
9. PERFORMING ORGANIZATION NAME AND ADDRESS Naval Research Laboratory Washington, D.C. 20375		10. PROGRAM ELEMENT, PROJECT, TASK AREA & WORK UNIT NUMBERS PME-106-41-058C- D3521
11. CONTROLLING OFFICE NAME AND ADDRESS Naval Electronics Systems Command Navy Space Projects Office (PME-106) Washington, D.C. 20360		12. REPORT DATE July 23, 1976 13. NUMBER OF PAGES 32
14. MONITORING AGENCY NAME & ADDRESS*(if different from Controlling Office)*		15. SECURITY CLASS. *(of this report)* Unclassified 15a. DECLASSIFICATION/DOWNGRADING SCHEDULE

16. DISTRIBUTION STATEMENT *(of this Report)*

Approved for public release, distribution unlimited.

17. DISTRIBUTION STATEMENT *(of the abstract entered in Block 20, if different from Report)*

18. SUPPLEMENTARY NOTES

This is a final report on this aspect of the overall problem; work on other aspects of the problem is continuing.

19. KEY WORDS *(Continue on reverse side if necessary and identify by block number)*

Antennas	Broadband antennas
Antenna arrays	Circularly polarized antenna elements
Aircraft antennas	VHF-UHF measurements

20. ABSTRACT *(Continue on reverse side if necessary and identify by block number)*

A broadband, circularly polarized antenna system suitable for use on WP-3 aircraft and operating in the VHF-UHF frequency region has been designed and fabricated. This airborne radiometer system will operate over a 3 to 1 frequency range without tuning. The installation contains a high- and low-frequency hemispherical coverage antenna and a high- and low-frequency fan-beam array. The entire installation is designed to fit into the standard APS-20

(Continued)

radome of the WP-3. Use has been made of a novel antenna element to achieve good pattern performance in such a confined space. Emphasis has been placed on low loss and reliable operation.

CONTENTS

VHF-UHF AIRCRAFT ANTENNA .

INTRODUCTION

An antenna system was designed and fabricated to be used in an airborne VHF and UHF radiometer system. This unusual radiometric antenna will operate without tuning over a 3 to 1 frequency band. The design incorporates two relatively high gain array antennas (14 to 20 dB gain) and two single radiating elements (5 to 8 dB gain). A general difficulty in regard to this task was that of isolating the antenna sufficiently from the aircraft structure to produce stable and predictable patterns.

To increase the isolation from the aircraft structure, the antenna is tilted downward relative to the aircraft wing and fuselage. Full azimuth coverage is obtained by flying the aircraft in a tight circle at a bank angle of 30 degrees. This places the peak of the antenna beam on the horizon. The type of radiating element employed in these antennas exhibits intrinsic directivity so as to further isolate the antenna beam from nearby reflecting surfaces.

ANTENNA LOCATION AND GENERAL DESCRIPTION

The WP-3 Lockheed Electra aircraft affords one reasonable location without airframe modification for the type of antenna system described in this report. The antenna is mounted within the radome that normally encloses the APS-20 radar antenna. The radome is located approximately 7 meters aft of the aircraft nose and immediately below the fuselage. Figures 1 through 3 depict the randome location. The radome is approximately 3.66 m in diameter, 1.22 m high, and has an elliptical cross section in the vertical plane.

The antenna system is designed to maximize its reflector surfaces within the confines of the existing radome and still perform its intended function. Two elliptically shaped

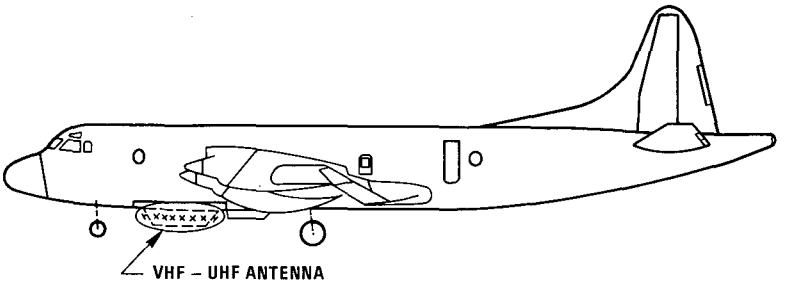

Fig. 1—WP-3 Aircraft, side view

Manuscript submitted April 22, 1976.

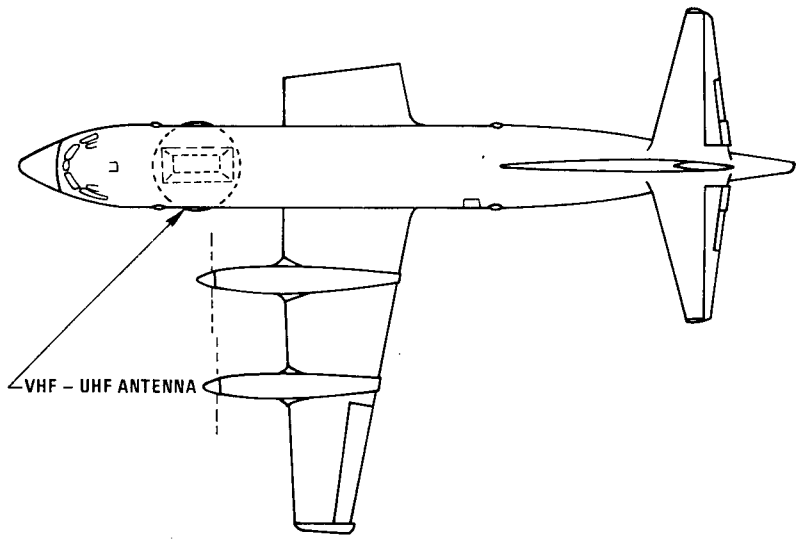

Fig. 2—WP-3 Aircraft, top view

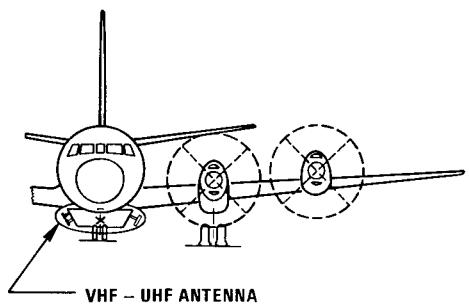

Fig. 3—WP-3 Aircraft, front view

flat reflectors (one facing port, the other facing starboard) are tilted 30 degrees from the vertical. The major axis of the antenna assembly lies parallel with the axis of the aircraft fuselage. The port antenna array operates over a range of from 200 to 350 megahertz (MHz) and the starboard array operates at from 342 to 600 MHz, affording an overlap of 8 MHz. These two arrays are separated by 1.22 m. Two single radiating elements are tilted downward by 45 degrees, one looking aft and the other looking forward. The aft radiating element covers the 200- to 350-MHz band; the forward-looking element covers the 342- to 600-MHz band. The port antenna array comprises one row of six circularly polarized crossed-dipole elements spaced 50.8 cm apart and mounted 29.2 cm above the reflector surface. The starboard antenna array comprises two rows of eight circularly polarized crossed-dipole elements spaced 29.65 cm apart, vertically and horizontally, and mounted 17.8 cm above the reflecting surface. Each radiating element is oriented 45 degrees with respect to the horizontal axis. This unusual orientation allows the elements to be more closely spaced than if they were arrayed with one arm of each element collinear with those of the adjacent elements. This close spacing makes possible proper control of the far out sidelobes for the required wide bandwidth. Figure 4 through 6 are sketches of the complete antenna system.

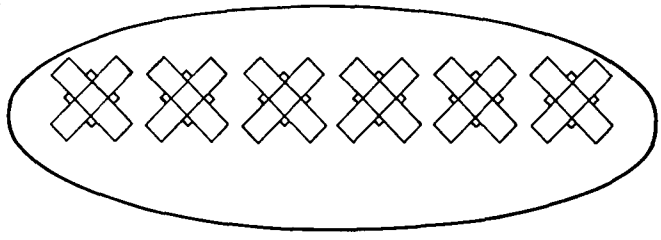

PORT ANTENNA ARRAY

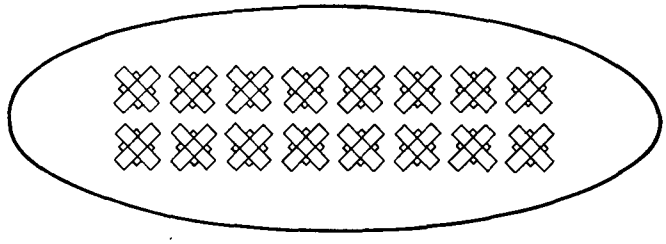

STARBOARD ANTENNA ARRAY

Fig. 4—Port and starboard arrays

FORWARD ANTENNA ELEMENT

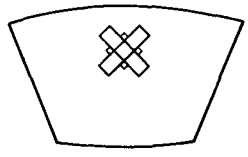

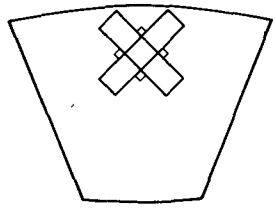

AFT ANTENNA ELEMENT

Fig. 5—Forward and aft antenna elements

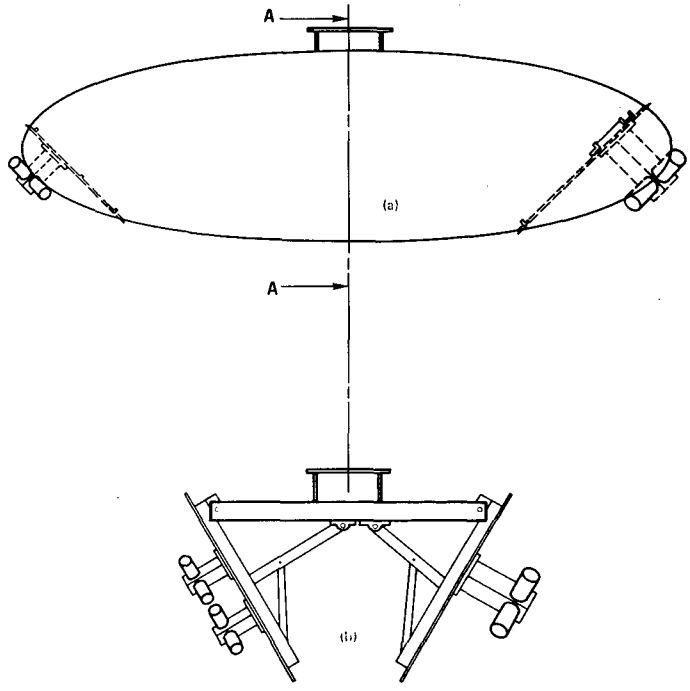

Fig. 6—Antenna assembly, cross-sectional views:
(a) side, (b) front, A-A

THEORY

A uniform feed amplitude is employed in the port and starboard antenna arrays in order to minimize the pattern beamwidth. Since the available space for radiating these frequencies is considerably less than ideal, minimizing the beamwidth will not only reduce reflection from the aircraft but will most efficiently make use of the available antenna area. The spacing between adjacent elements is the greatest possible without allowing a significant increase in the near or farout sidelobe structure. This consideration resulted in a spacing of 0.593λ at the highest operating frequency and an electrical spacing of 0.339λ at the lowest operating frequency for each array. The physical spacings are thus 29.64 and 50.8 cm for the starboard and port arrays, respectively. The close electrical spacing at the lower frequencies dictates that some measure of control over the mutual coupling must be exercised. This control is provided by a number of isolated hybrid ports, distributed throughout the feed network, which absorb out-of-phase reflected energy.

The low band antenna array, with a 50.8-cm spacing, provides enough area for a single row of six crossed dipole radiators. The far-field antenna pattern in the horizontal plane may be represented mathematically by the following equation:

$$G(\theta) = A(\theta) \times E(\theta) , \tag{1}$$

where $E(\theta)$ represents the element pattern as a function of azimuth angle, and $A(\theta)$ represents the array factor as a function of azimuth angle. Furthermore, the array factor is given by

$$A(\theta) = \cos(\psi/2) + \cos(3\psi/2) + \cos(5\psi/2) \tag{2}$$

$$\psi/2 = \frac{180\,d}{\lambda}(\sin\theta),$$

where

θ = azimuth angle measured from broadside,

d = element spacing

λ = operating wavelength.

The element pattern must account for the feed gap in each set of dipole elements and for the effect of the spacing of the dipole elements from the reflector. Thus,

$$E(\theta) = \cos\left(\frac{\pi g}{\lambda}\sin\theta\right) \times \sin\left(\frac{2\pi\ell}{\lambda}\cos\theta\right) \times \frac{\cos(\pi/2\sin\theta)}{\cos\theta}, \tag{3}$$

in which g = distance between the gaps, and ℓ = distance above the reflector surface. Equation (1) is plotted in Figs. 7 and 8 to show the calculated horizontal and vertical patterns, respectively, of the low-band array. Since this antenna is only one element high in the vertical plane, it has an array factor of unity in that plane. Therefore, Fig. 8 is also a plot of Eq. (3) and represents the horizontal or vertical pattern of a single element. It will be noted in Fig. 8 that the element beam is broader at 350 MHz than at 200 MHz. This is to be expected after examination of the second factor in Eq. (3).

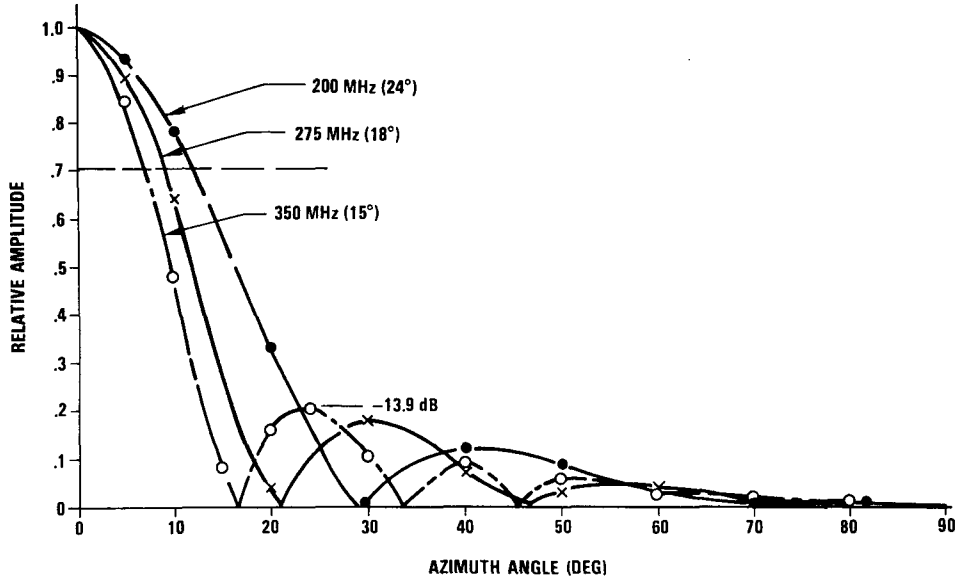

Fig. 7—Horizontal antenna pattern, low-band fan beam from 1 × 6-element array of crossed dipoles

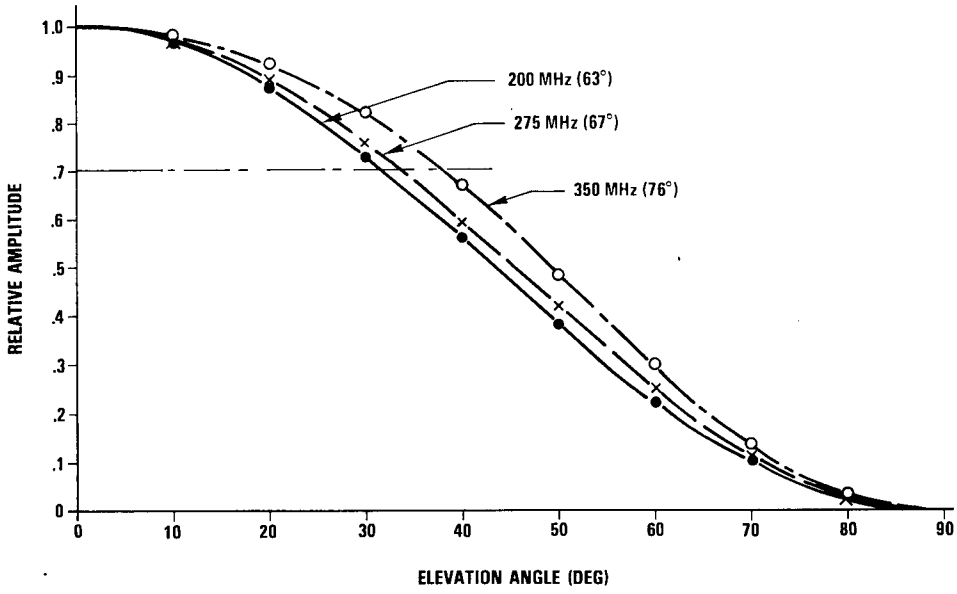

Fig. 8—Vertical antenna pattern, low-band fan beam from 1 X 6-element array of crossed dipoles

The horizontal array factor for the high-frequency array is

$$A(\theta) = \cos(\psi/2) + \cos(3\psi/2) + \cos(5\psi/2) + \cos(7\psi/2), \quad (4)$$

and the element pattern is represented by Eq. (3) with different values for g and ℓ.

The vertical array factor for this antenna is

$$A(\theta) = \cos(\psi/2). \quad (5)$$

Equation (1) is plotted in Figs. 9 and 10 showing the horizontal and vertical patterns for the high-band array. In this array the reflector provides sufficient area for two rows of eight elements. Notice that the change of beamwidth with frequency in the vertical plane of this array is opposite to that of the low-band array shown in Fig. 8. This is because the array factor overpowers the effect of ground-plane spacing.

THE RADIATING ELEMENT

The radiating element chosen for this antenna system was designed under Contract N00173-75-C-0513. It is a dual-polarized broadband dipole element containing four widely separated gaps. Each collinear pair of arms is fed by a 180-degree balun. Figures 11 and 12 are photographs of the low-band and high-band dipoles used in the antenna system. The widely separated dipole gaps provide inherent element directivity not present in standard dipole designs. Each dipole is required to operate over a 1.75:1 frequency band. However, these elements have the capability of producing good patterns over a 3.3:1 frequency band [1].

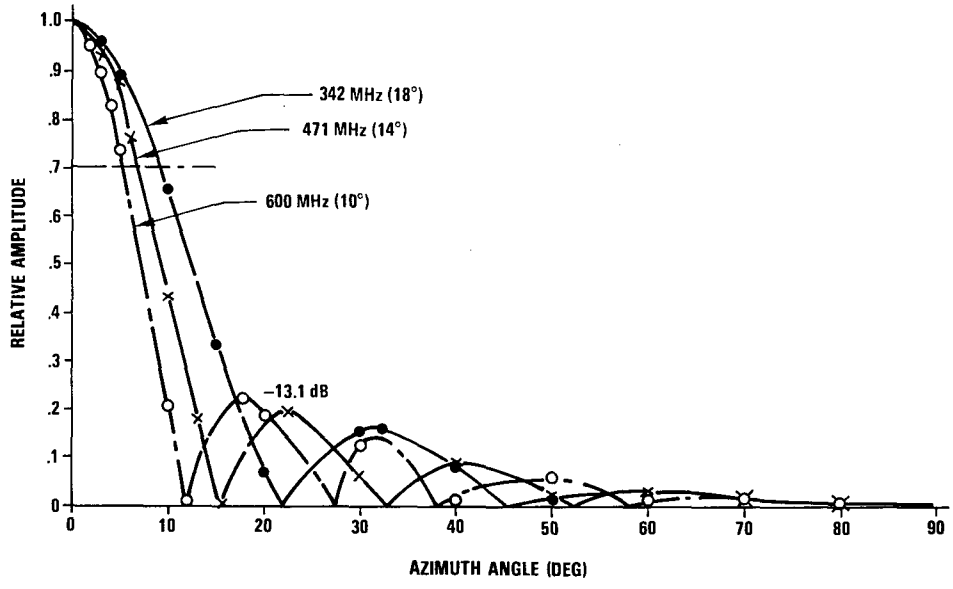

Fig. 9—Horizontal antenna pattern, high-band fan beam from 2 × 8-element array of crossed dipoles

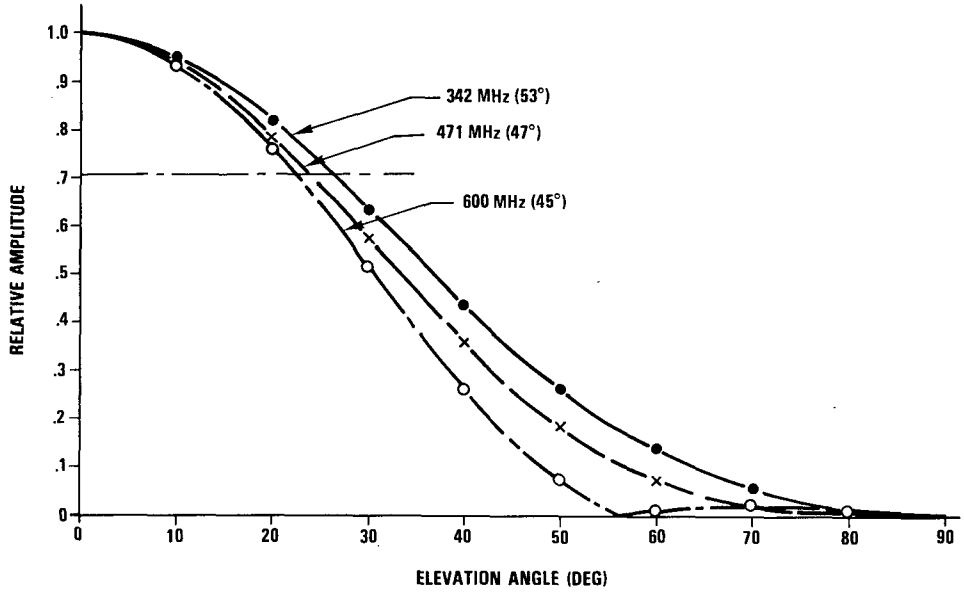

Fig. 10—Vertical antenna pattern, high-band fan beam from 2 × 8-element array of crossed dipoles

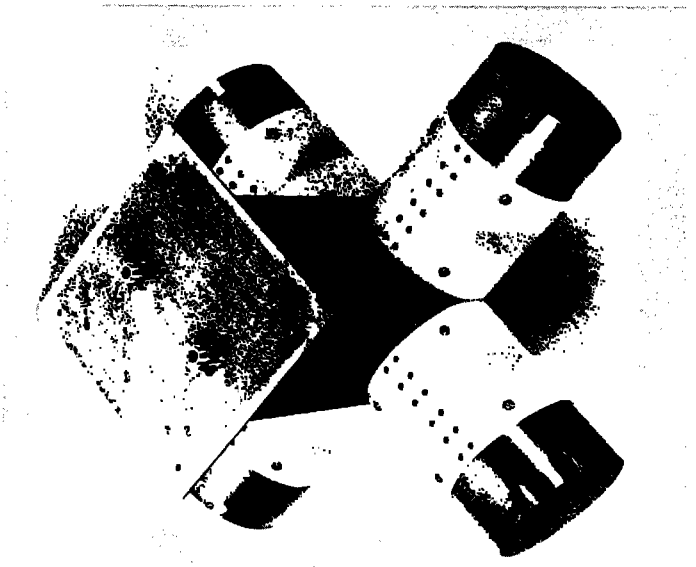

(a) rear view

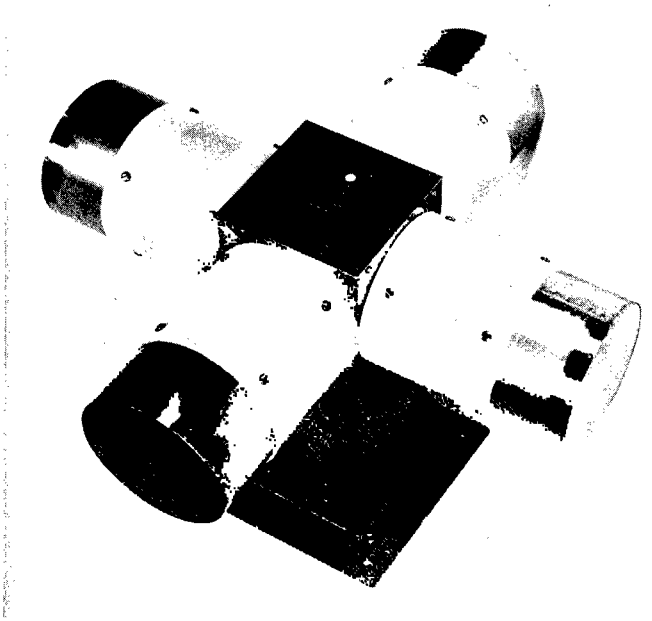

(b) front view

Fig. 11—Low-band dual-polarized dipole element

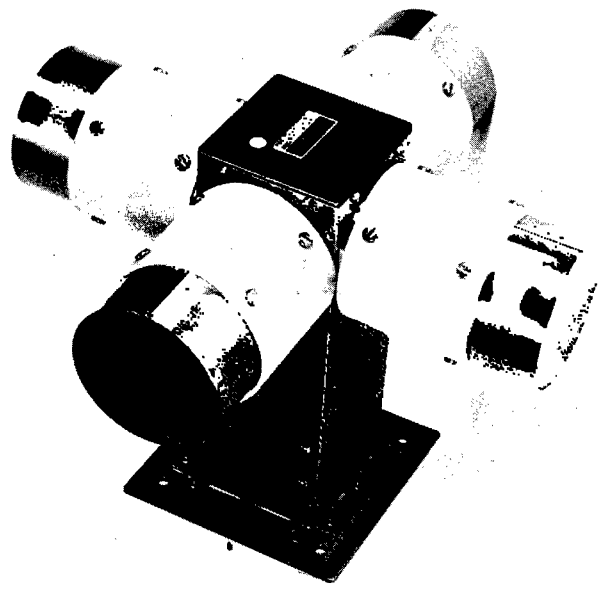

(a) front view

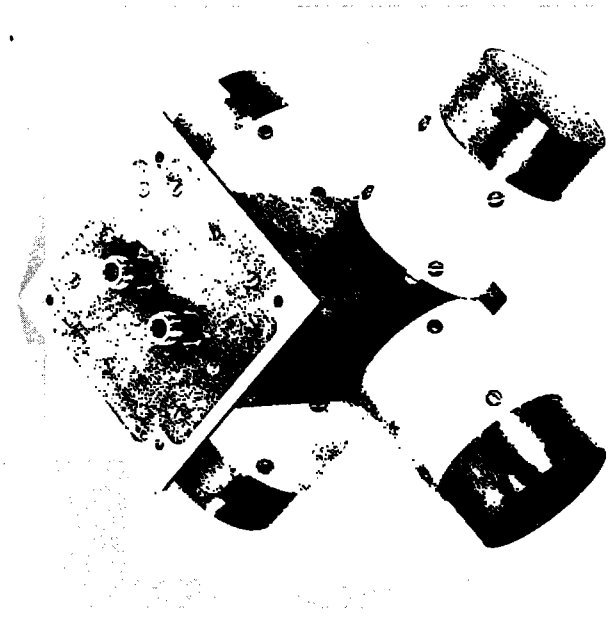

(b) rear view

Fig. 12—High-band dual-polarized dipole

Both elements are constructed of 0.381-mm stainless steel. The support shaft is square in cross section, and each of the four radiating arms is cylindrical. The gaps are flared and shaped in order to control the gap impedance over the wide frequency range of operation.

The low-band dipole is 35.6-cm high, has an arm length of 48.26 cm, and weighs 3.15 kg (7 lb). The high-band element is 22.9-cm high, has an arm length of 29.2 cm, and weighs 1.8 kg (4 lb). In the frequency range of interest the low-band dipole input VSWR varies from 1.6:1 to 2.0:1, and its calculated losses are 0.4 to 0.7 dB. The high-band dipole exhibits a 1.5:1 to 1.8:1 input VSWR, and its losses are 0.3 to 0.5 dB. Figures 13 and 14 show the *E*- and *H*-plane element patterns for the low-band element, and Figs. 15 and 16 show the corresponding patterns for the high-band element. These patterns were measured over a 0.914-m by 1.22-m ground plane by the Alford Manufacturing Company. The high-band element patterns show a partial main-beam breakup at 500 MHz and above. This comes about because the height of the element above the ground is approximately 25 mm (1 in.) too great.

Measurements of boresight circularity taken at the dipole manufacturer's plant are listed in Table 1.

ANTENNA SYSTEM RF NETWORK

Figure 17 is an RF block diagram of the antenna system. Noise signals go to the dual-polarized crossed-dipole elements and are resolved into two orthogonal signals. These signals then pass through a 90-degree, 3-dB hybrid in such a manner as to produce a right-hand circularly polarized output. Out-of-phase and unbalanced signals are absorbed by a 1/8-w resistor located in the cancellation arm of the 3-dB quadrature hybrid. In the cases involving the port and starboard arrays, the noise signals are fed through equal lengths of RF cable and summed at the output of a power divider network. The signal from each array is then fed to a diode switch which can be operated remotely to select the desired

Table 1—Element Boresight Circularity

Frequency (MHz)		Axial Ratio (dB)
Low Band	200	1.0
	250	0.6
	300	1.0
	350	1.0
High Band	342	1.3
	400	2.7
	500	2.3
	600	1.7

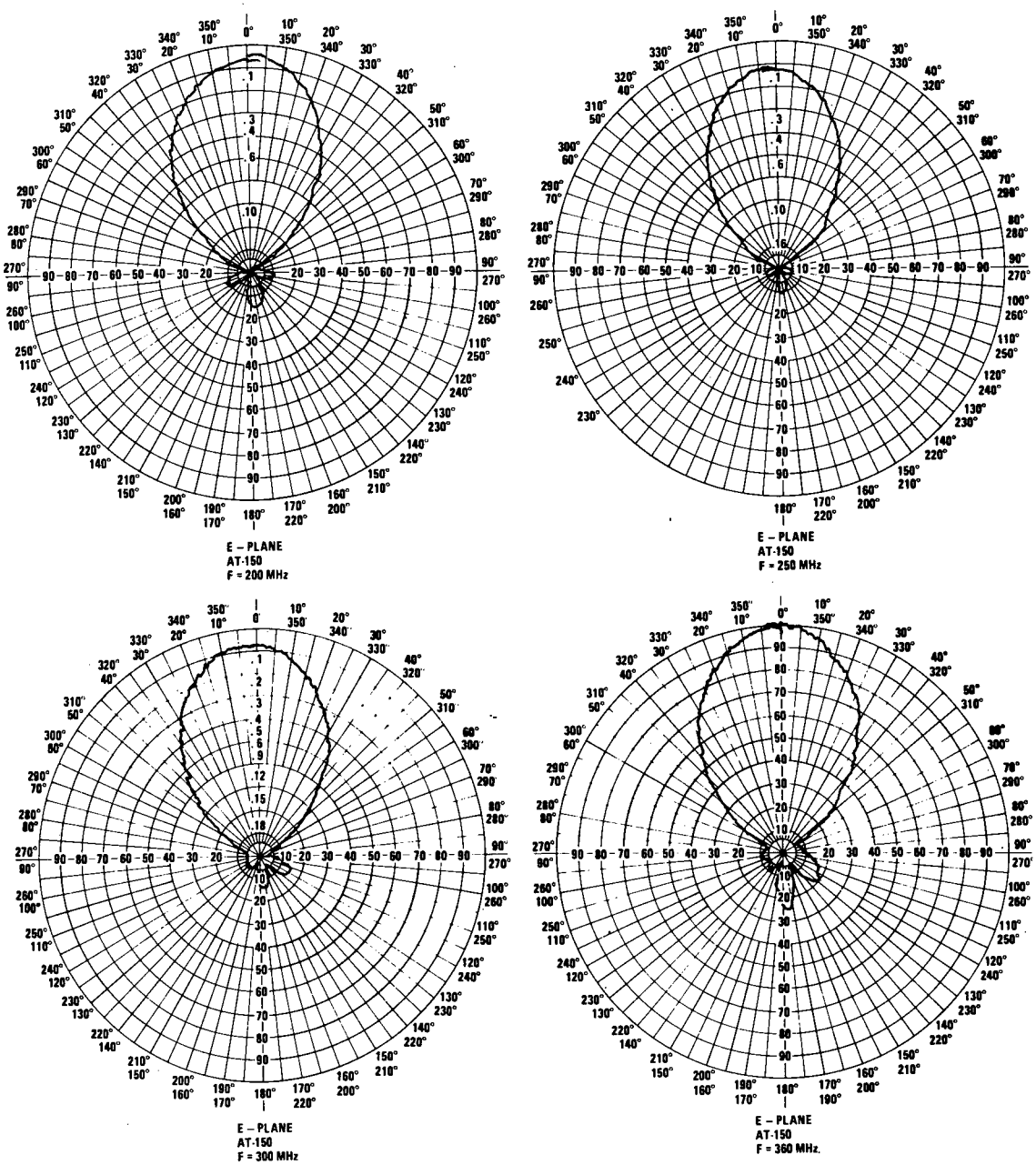

Fig. 13—Low-band *E*-plane element patterns

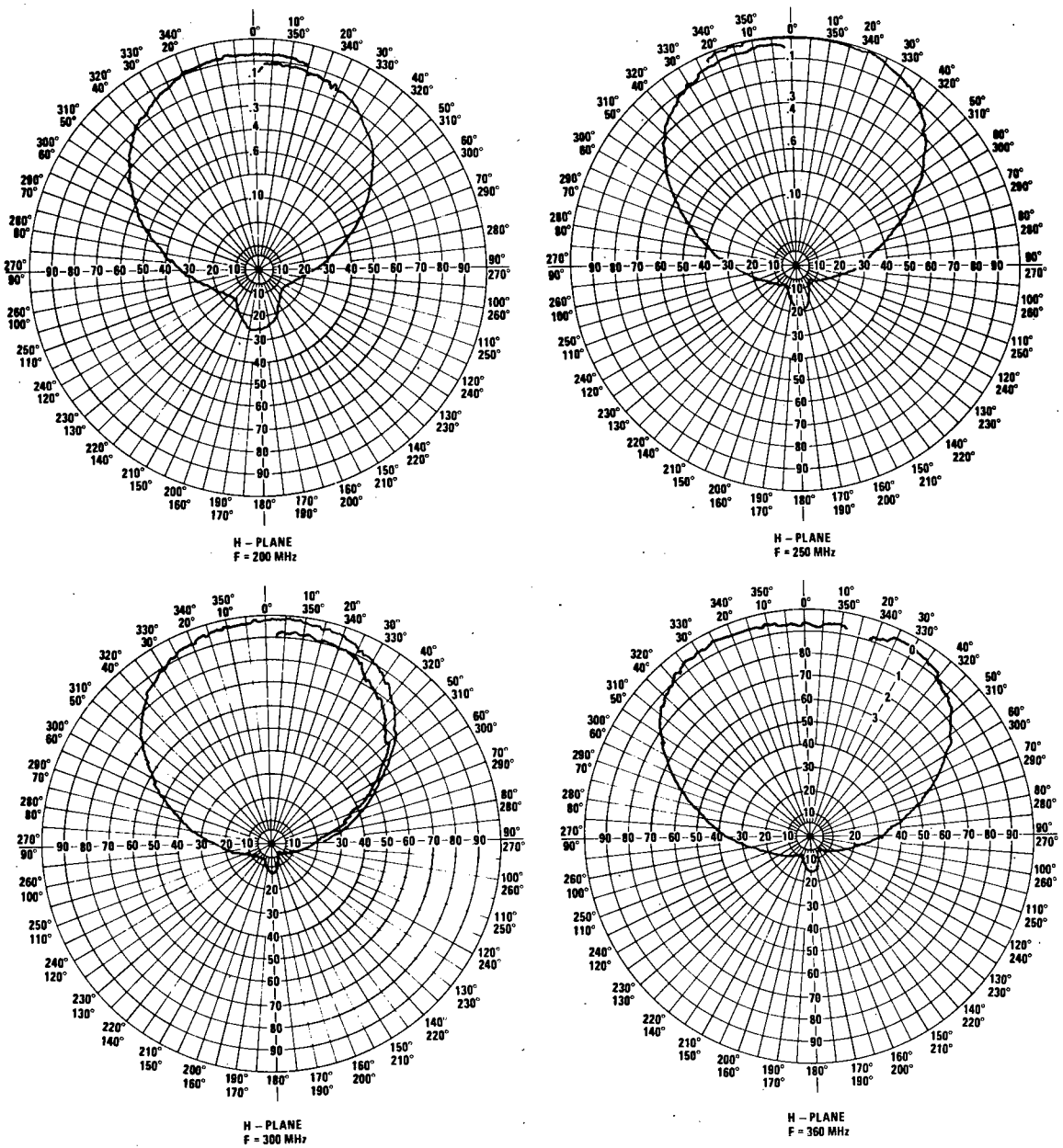

Fig. 14—Low-band *H*-plane element patterns

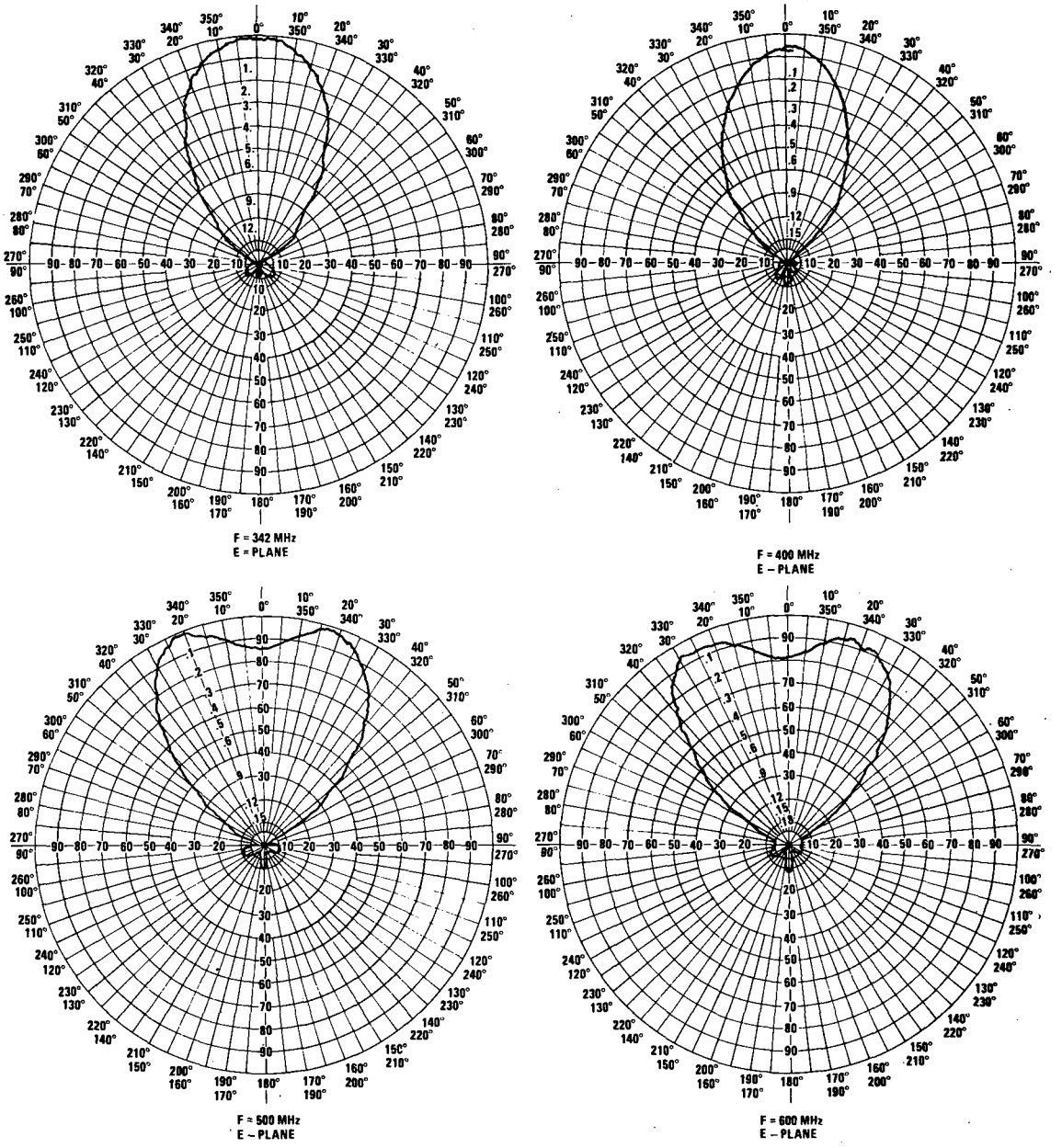

Fig. 15—High-band *E*-plane element patterns

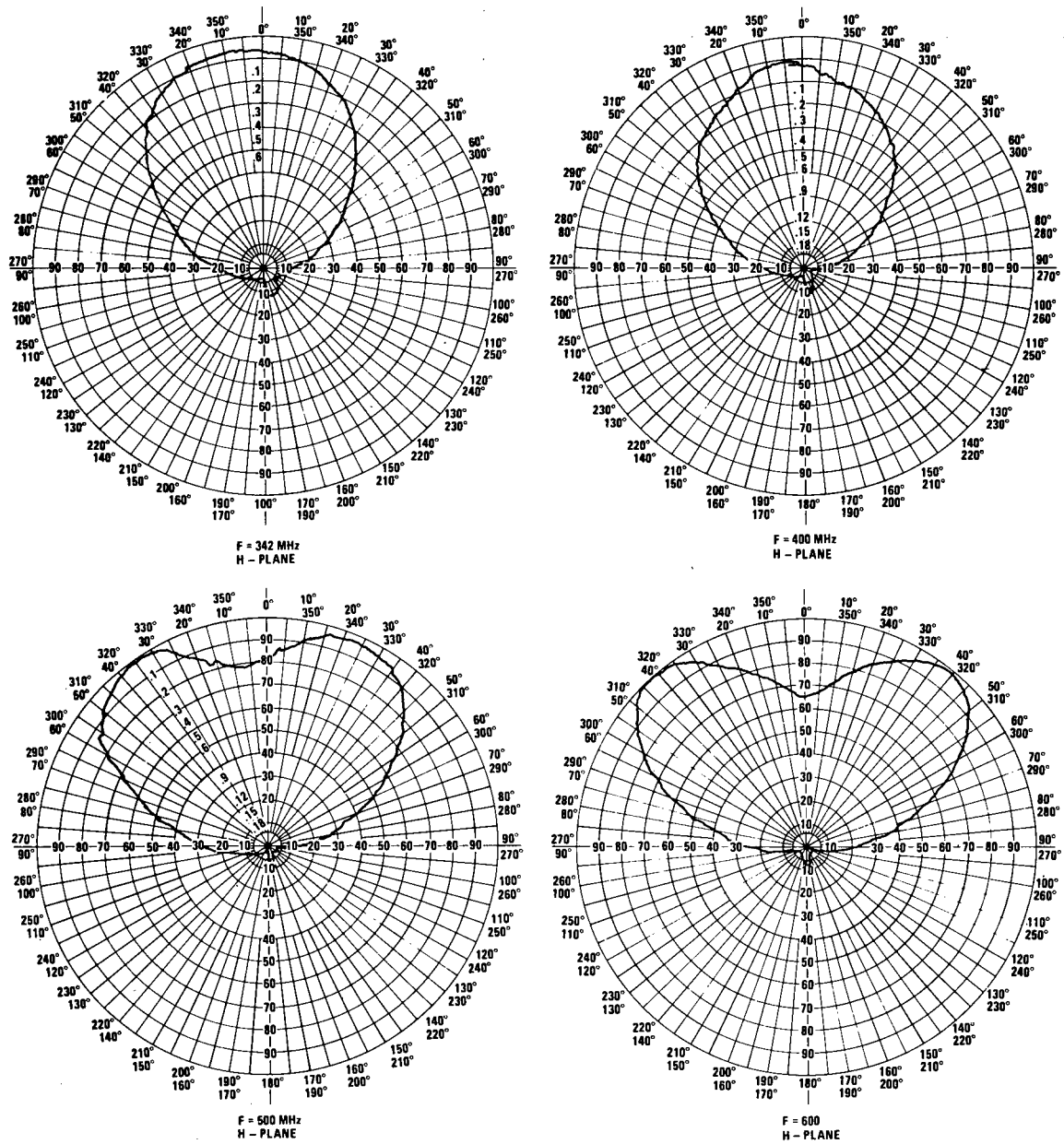

Fig. 16—High-band *H*-plane element patterns

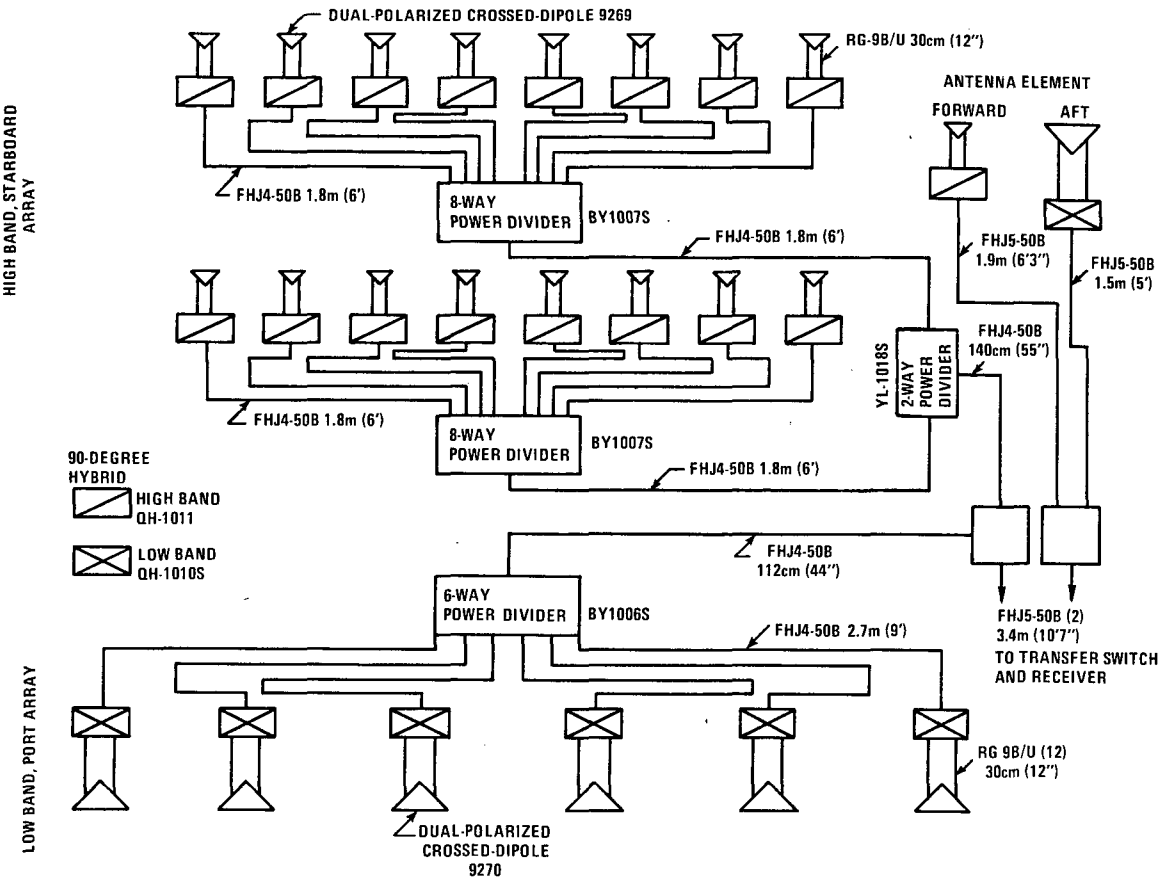

Fig. 17—Antenna system RF block diagram

frequency band. The circularly polarized signals from the forward and aft single antennas are sent to another diode switch that is used to select either the port or the starboard antenna.

MECHANICAL STRUCTURE

The supporting structure for the arrays was fabricated from aluminum sheets and tubing; welding and riveting techniques were employed throughout. The structure consists of five major areas: the high-band array reflector, the high-band single-element reflector, the low-band array reflector, the low-band single-element reflector, and the interconnecting framework. The high- and low-band reflector surfaces, which are elliptical in shape, are constructed of 0.813-mm 6061-T6 aluminum sheet. They each comprise 3.1 m^2 of surface area, with the minor axis 1.14 m long and the major axis 3.45 m long. The high-band single element reflector, trapezoidal in shape, contains 0.613 m^2 of surface area (0.63 m high by a maximum of 1.22 m wide). The low-band single element reflector contains 0.855 m^2 and is 0.86 m high by a maximum of 1.35 m wide. The interconnecting structure consists of aluminum tubing and prefabricated channels and serves to provide a rigid framework for holding the reflectors in place. Additional prefabricated channels

are used as strengthening members behind each radiating element. The completed antenna system weighs 159 kg (350 lb).

MODEL MEASUREMENTS

A scale model of the low-band antenna array was constructed to simulate this array at its center frequency. The array was mounted in a 1/18th scale model of the C-121 aircraft. This aircraft, in the forward region, is similar to the WP-3 in many respects. The scaled frequency of 5186.5 MHz corresponds to 275 MHz, full scale. Vertical and horizontal patterns of this scale-model antenna array agree closely with the calculated values for the beamwidths (within 2 degrees). Measurements taken of the array mounted on the aircraft indicate a 13° (19%) narrowing of the 3-dB beamwidth in the vertical plane and a 1° (5%) narrowing in the horizontal plane. First sidelobe levels increased approximately 3 dB, and pattern ripple increased 1½ dB in the vertical plane. These distortions are attributed to the effects of aircraft structure. An additional 1.5-dB pattern distortion is due to the effects of propeller modulation upon the vertical antenna pattern.

TESTING THE ANTENNA SYSTEM

The complete antenna system was mounted in the inverted position above an MP-88 antenna pedestal located on the roof of Building 208 at NRL. A log periodic antenna connected to a transmitter was mounted on the top of a 6.7-m tower, 42.7 m away, to complete the antenna measurement range. This antenna range, far from ideal, was the only test range that was readily available. Figures 18 through 21 show the azimuth and elevation antenna patterns of the low-band array; Figs. 22 through 25 depict the high-band array patterns. Elevation patterns for all bands cover only 90 degrees because of pedestal limitations. All patterns were measured for right-hand circular polarization. Table 2 summarizes the 3-dB beamwidths, first sidelobe levels, and directive gains for each array. The characteristics of the single-element ("hemispheric") antennas are summarized in Table 3.

The input voltage standing wave ratio (VSWR) was measured for both antenna arrays. These measurements, referenced to a 50-ohm impedance, are summarized in Table 4.

The intended application of these antennas for measuring VHF-UHF noise required an accurate assessment of the losses and reflections in the antenna system. Measurement of the losses in the feed networks was accomplished by replacing the elements with matched 50-ohm loads. The forward and reverse power at the input to the feed network and the power delivered to a typical output port were then measured. From these measurements the input VSWR and the absorption loss of the feed network were determined. Table 5 summarizes these absorption losses for the feed networks of both the high-band and low-band arrays.

The effective reflection coefficient of each array was measured in the following manner. The feed network was reconnected to the radiating elements, except that the feed line to one of the elements was replaced with a dual-directional coupler and a suitable short length of cable. The length of this cable was carefully selected so that the path length, which included the directional coupler, exactly matched the electrical length of the cable

Fig. 18—Low-band array antenna pattern at 200 MHz

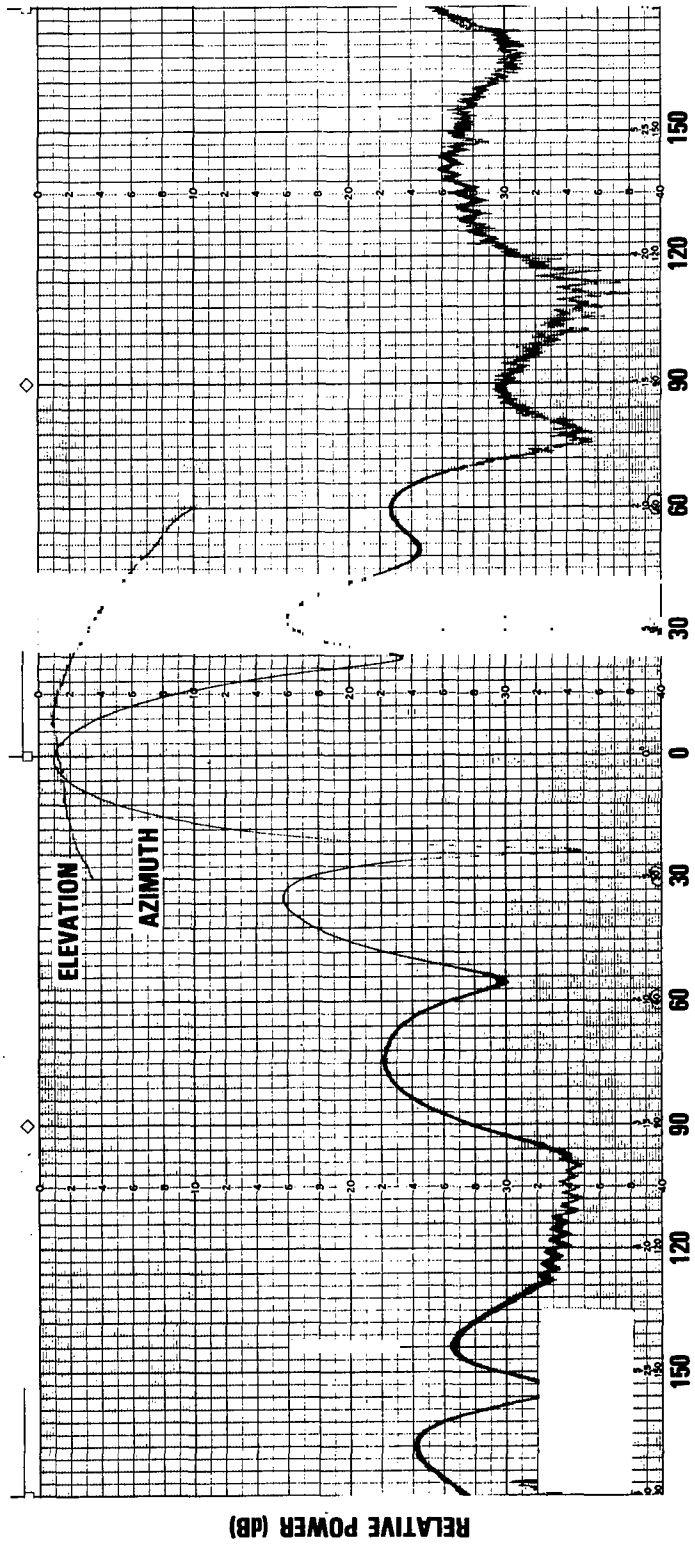

Fig. 19—Low-band array antenna pattern at 248 MHz

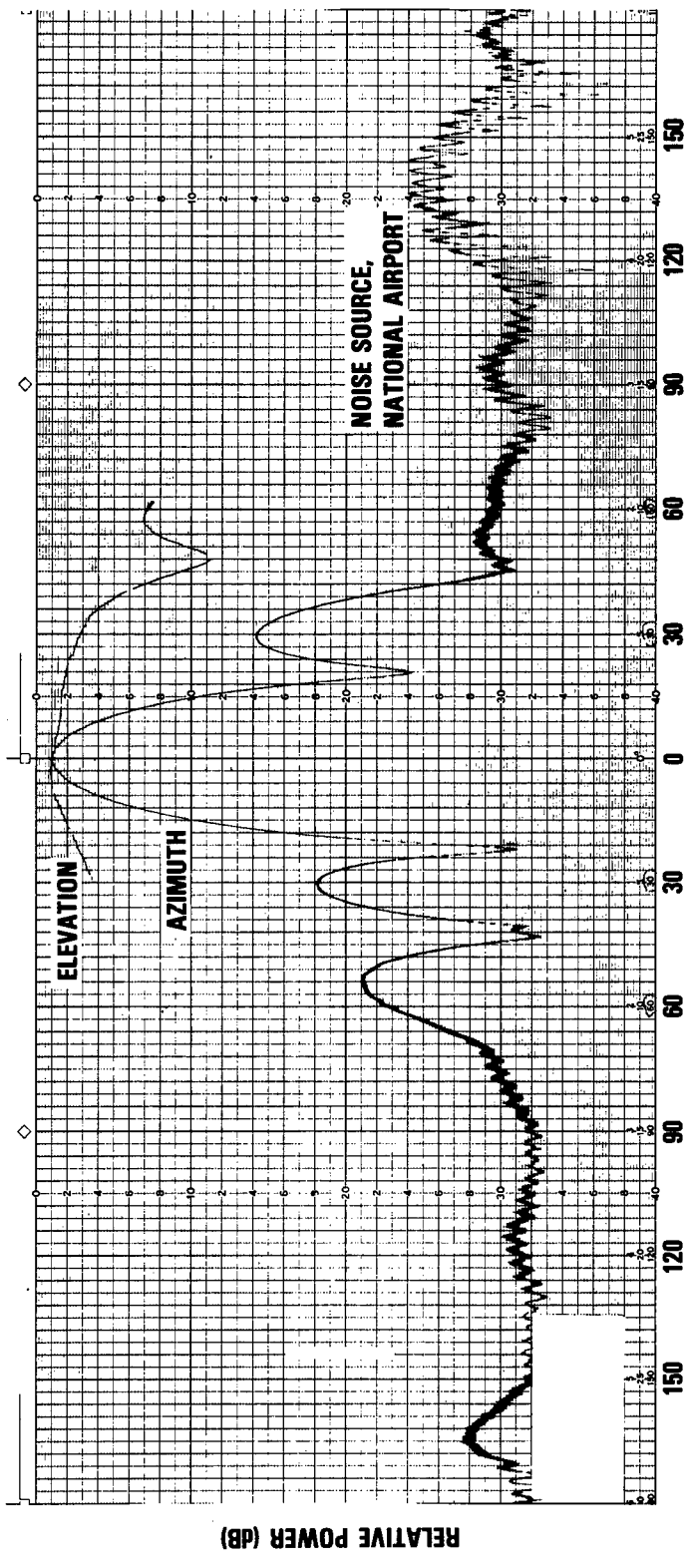

Fig. 20—Low-band array antenna pattern at 275 MHz

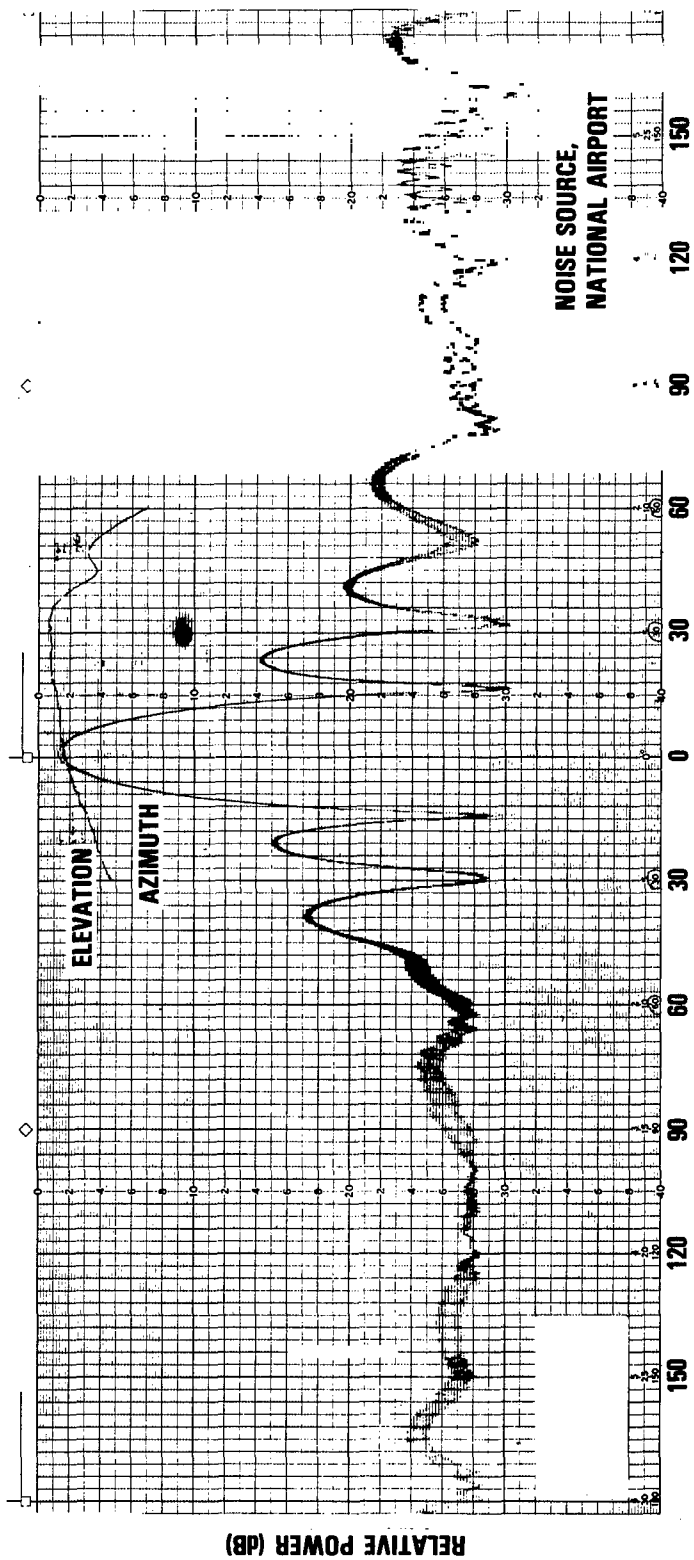

Fig. 21—Low-band array antenna pattern at 349 MHz

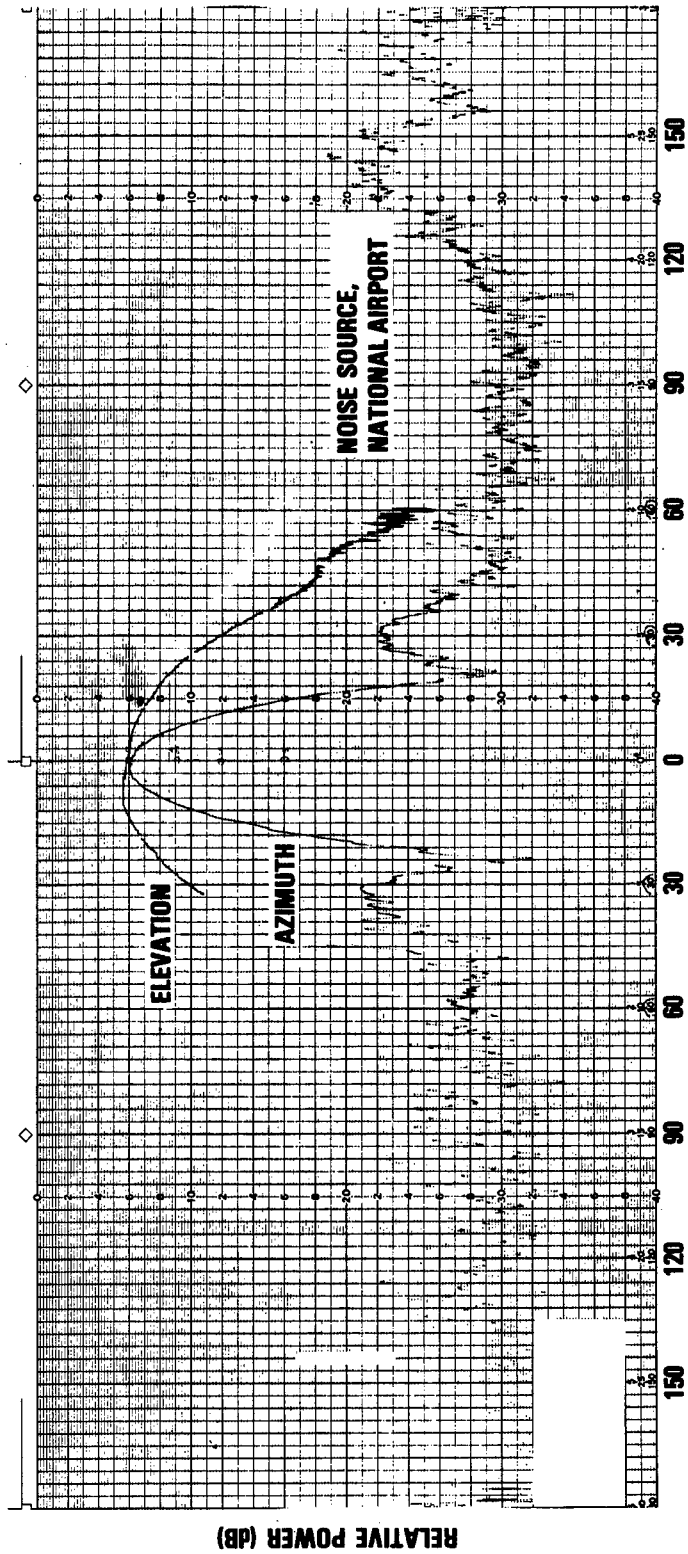

Fig. 22—High-band array antenna pattern at 344 MHz

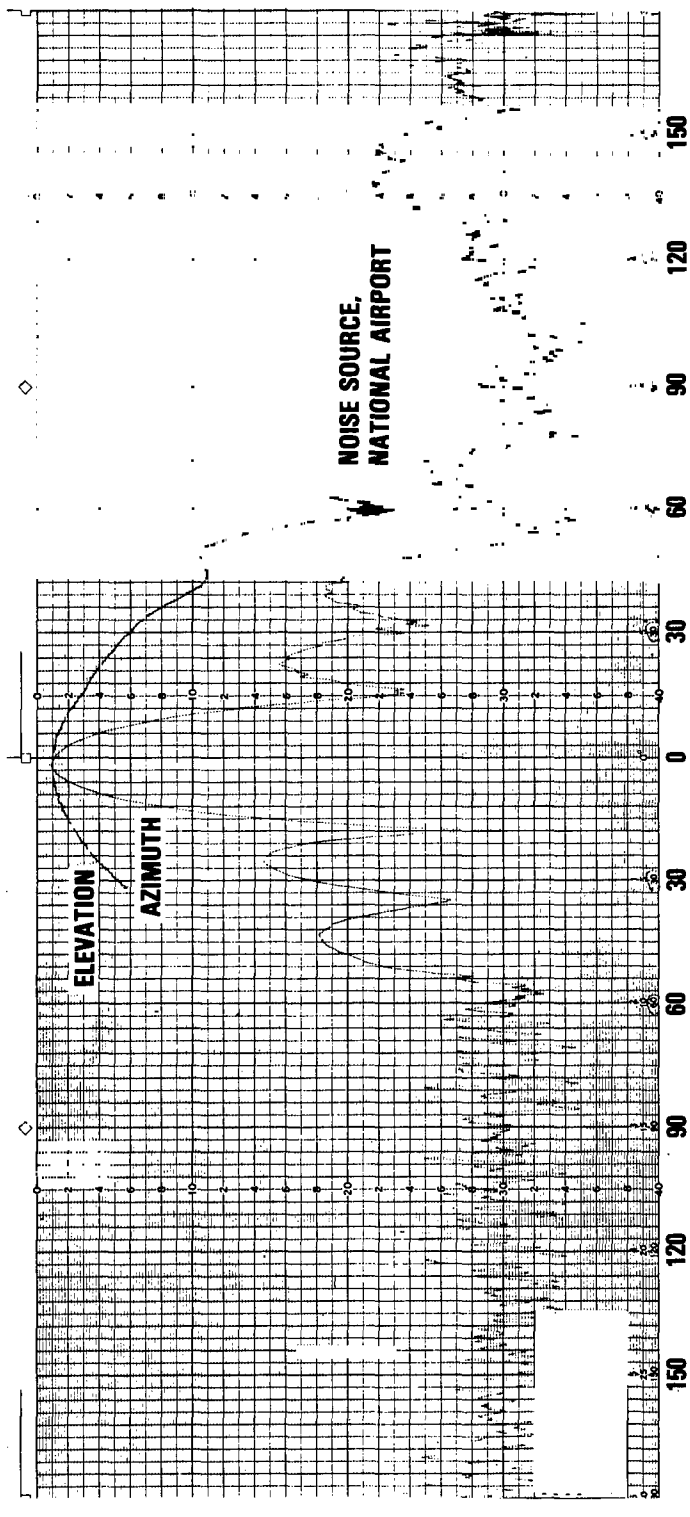

Fig. 23—High-band array antenna pattern at 434 MHz

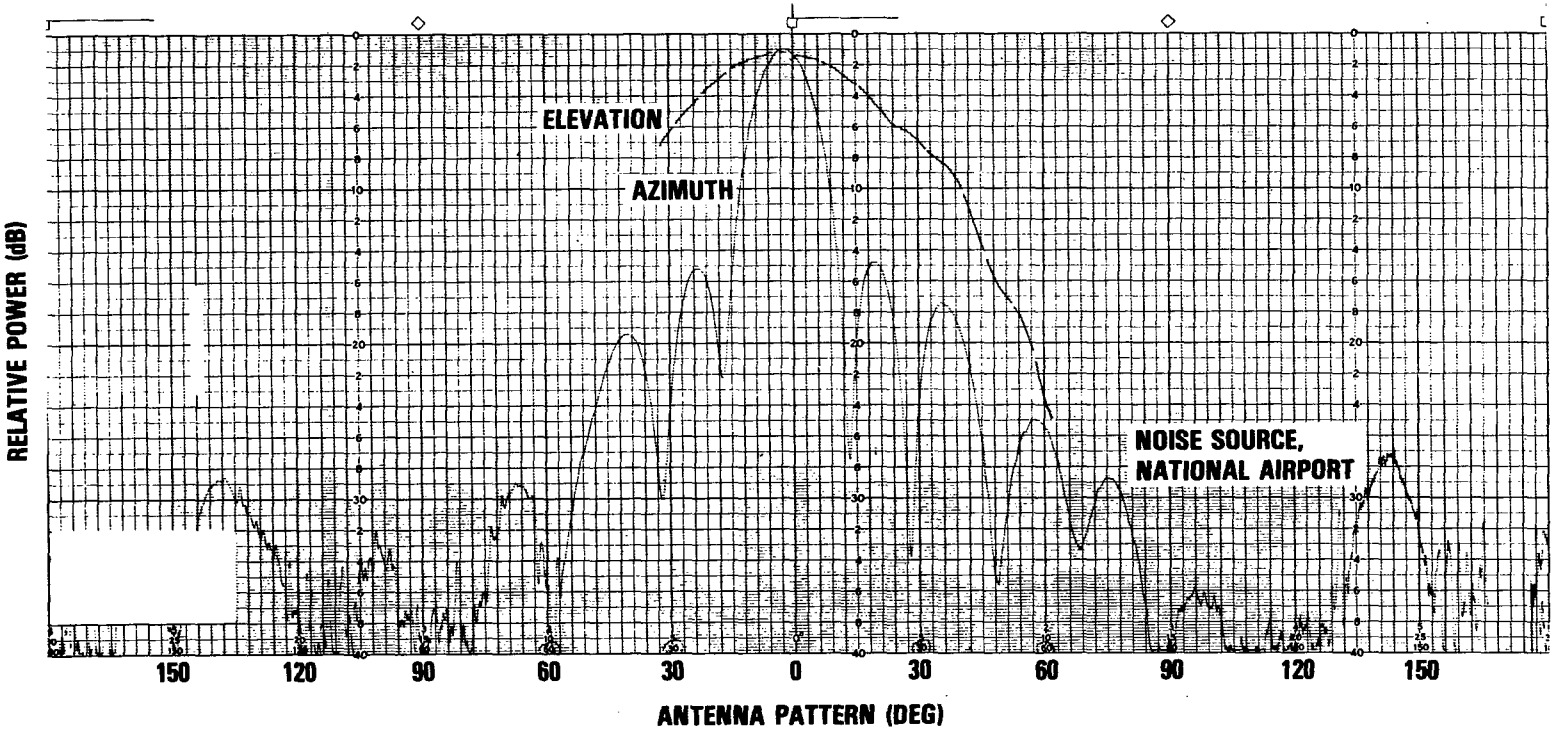

Fig. 24—High-band array antenna pattern at 471 MHz

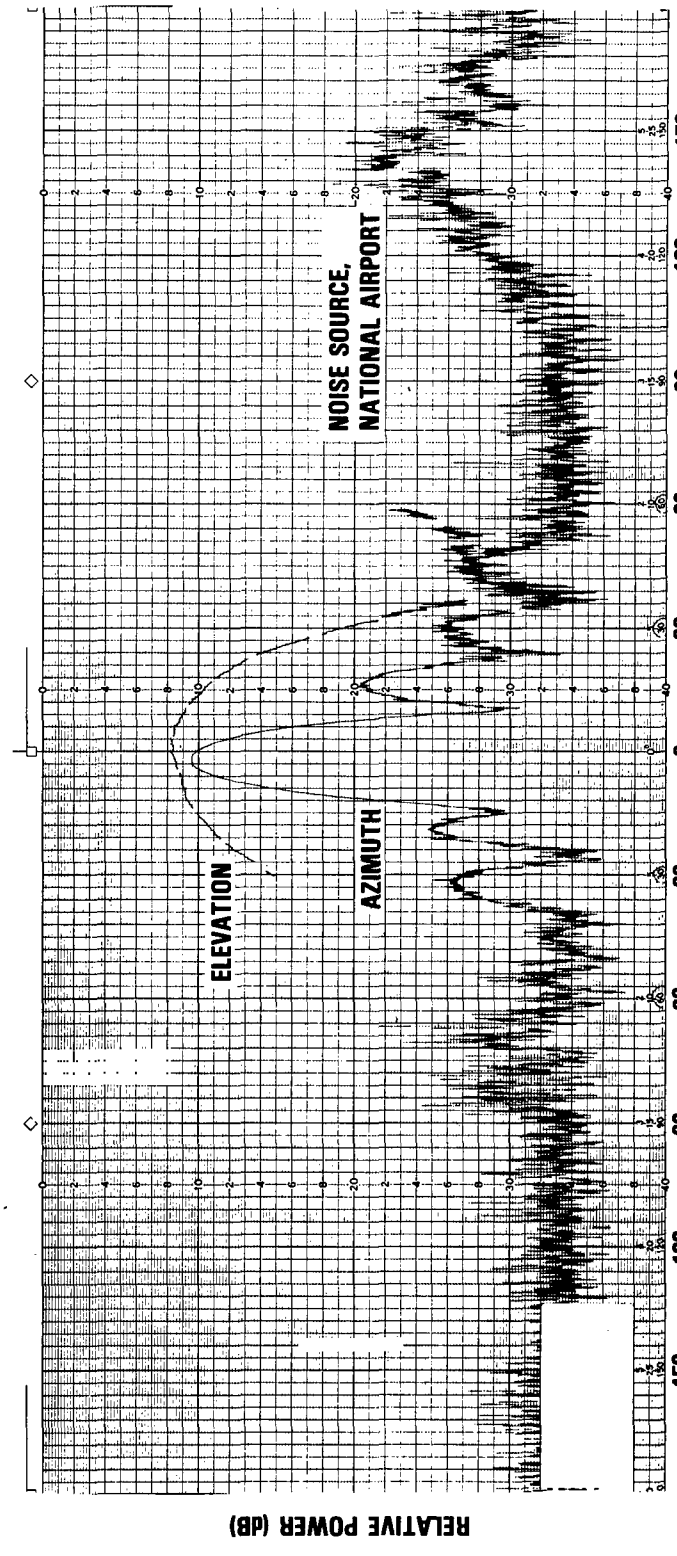

Fig. 25—High-band array antenna pattern at 600 MHz

Table 2—Antenna System Array Characteristics

Frequency (MHz)	3-dB Beamwidths		1st Sidelobe	Directive Gain
	Azimuth (deg)	Elevation (deg)	Peak	
			(dB)	(dB)
Low-Band Array				
200	24.5	63	-19.4	14.3
226	22.0	63	-14.8	14.7
248	20.0	66	-14.9	14.9
275	18.0	68	-15.2	15.3
349	14.0	74	-13.4	16.0
High-Band Array				
342	18.0	47.5	-15.5	16.8
434	15.0	47.5	-14.1	17.6
456	13.5	43.0	-13.8	18.5
471	13.5	41.5	-14.0	18.7
534	12.0	42.0	-12.4	19.1
600	11.5	39.0	-13.2	19.6

Table 3—Hemispheric Antenna Characteristics

Frequency (MHz)	3-dB Beamwidths	
	Azimuth (deg)	Elevation (deg)
Low-Band Element		
226	83	57
248	58	55
349	74	47
High-Band Element		
349	41	51
439	67	55
540	76	50

Table 4—Antenna Array Input Standing Wave Ratio

Low Band		High Band	
Frequency (MHz)	VSWR	Frequency (MHz)	VSWR
226	1.5	349	1.2
243	1.3	434	1.7
248	1.4	439	1.6
349	1.6	540	1.1

Table 5—Array Network Absorption Losses

Low Band		High Band	
Frequency (MHz)	Loss (dB)	Frequency (MHz)	Loss (dB)
226	0.70	349	1.75
243	0.85	434	1.83
248	0.95	439	1.91
349	1.00	596	2.04

that it replaced. In this way the electrical balance of the array was maintained for the measurement. Measurements of forward and reverse power at the network/element interface were made in this manner for a typical central element and for a typical end element. Simultaneously, the input power to the entire feed network was measured. From these measurements, the total radiated and reflected power (and hence the effective reflection coefficient) for each antenna were determined. Table 6 shows the results of these measurements in terms of the VSWR at the antenna face for each array.

The combined effects of both reflection and absorption losses for the two antennas are shown in Table 7. The figures shown here represent the net loss for a signal at the

Table 6—Effective VSWR at the Array Face

Low-Band Array		High-Band Array	
Frequency (MHz)	VSWR	Frequency (MHz)	VSWR
226	1.95	349	1.55
243	1.80	434	1.44
248	1.73	439	1.49
349	1.38	596	1.39

Table 7—"Active" Array Losses

Low Band		High Band	
Frequency (MHz)	Loss (dB)	Frequency (MHz)	Loss (dB)
226	2.27	349	2.16
243	1.91	434	1.66
248	2.00	439	1.63
349	2.91	540	1.33

input port of each antenna. Comparison of Table 7 with Table 5 indicates that the mismatch at the network/element interface (which includes the effects of mutual coupling in the active array) has increased the losses of the low-band antenna array by 1.0 to 1.9 dB. In the case of the high-band array, the losses have apparently decreased by 0.17 to 0.71 dB at 434 MHz and above, possibly because of fortuitous phasing of the reflections from the elements. At 349 MHz on the high-band array, however, the loss has increased by 0.41 dB. This effect can be attributed to differences in the electrical path lengths in the feed networks. It is known that the electrical path lengths are approximately a half wavelength longer in the high-band array. It should be possible to optimize the power transfer in the array (over the frequency band) by suitable selection of the feed-network path lengths. However, this was not attempted. It is relevant to point out, that the measurement accuracy is on the order of ±1.0 dB. Since it is not possible for the "active" array losses to be less than the measured network absorption loss, measurement error is attributed to this discrepancy.

Table 8 lists results of measurements made on individual components of the RF feed network of the VHF-UHF antenna system.

Table 8—Data on Components of RF Feed Network

Component	Test Freq. (MHz)	Phase Diff. (Deg ±)	Ampli. Diff. (dB)	Insertion Loss (dB)	Input VSWR	Isol. Min (dB)
RG-214/U Cables—30 cm (12")	600	5.4	–	0.10	1.10	–
FHJ4-50B Cables—2.7 m (9')	350	3.8	–	0.20	1.05	–
FHJ4-50B Cables—1.8 m (6')	600	7.2	–	0.10	1.08	–
90° Hybrids, high band	600	4.0	0.35	0.17	1.13	35.0
90° Hybrid, low band	350	1.0	0.20	0.04	1.09	39.0
2-Way power divider	600	0.3	0.10	0.17	1.30	16.2
8-Way power dividers	600	4.0	0.70	0.38	1.50	17.1
6-Way power divider	350	6.1	1.10	0.95	1.50	15.0

SUMMARY OF ANTENNA ARRAY PERFORMANCE

Figure 26 shows the measured half-power beamwidth for the azimuth and elevation planes of the low-band and high-band arrays at right-hand circular polarization. Calculated values of directive gain are plotted as a function of frequency in Fig. 27. The measured half-power beam-widths were used in the gain calculations. The measured overall losses (as given in Table 7) were subtracted from the calculated directive gain to arrive at the net array gain. Thus, the net gain of the array includes the effects of mutual coupling as well as the loss due to the feed network. The resulting antenna efficiencies range from a low of 51% to a maximum value of 69%. Also, in Fig. 27, the network absorption loss is plotted as a function of frequency. Notice that above 500 MHz the network loss is 0.4 dB greater than the difference between the directive gain curve and the net gain curve. This discrepancy is well within the measurement accuracy.

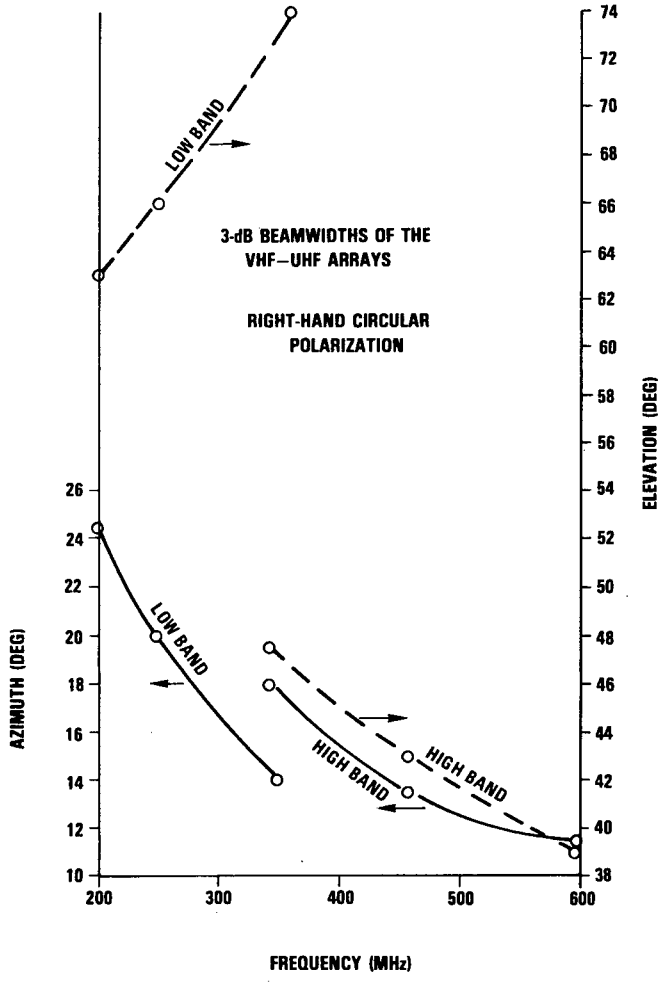

Fig. 26—Three-decibel beamwidths of the VHF-UHF arrays; right-hand circular polarization

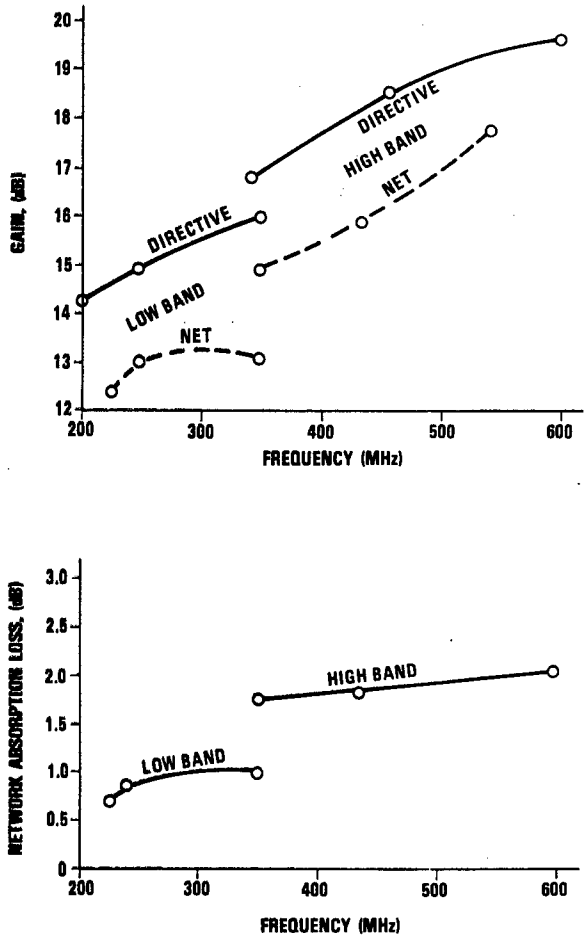

Fig. 27—Directive and net gains of the VHF-UHF antenna arrays

ACKNOWLEDGMENTS

I would like to give credit to J. Titus and his staff for their excellent mechanical engineering design of the antenna system, to J. Devine, L. Gasch, and to N. Pollack for their assistance in assembling and testing this system, and to the members of the Microwave Techniques Branch for their generous lending of their antenna test factilities.

REFERENCE

1. United States Patent 2,844,818, July 22, 1958, Andrew Alford, Cambridge, Mass.

*U.S. GOVERNMENT PRINTING OFFICE: 1976 211-264/594 1-3